Journal of Magnetism and Magnetic Materials 471 (2019) 394–399

Contents lists available at ScienceDirect

Journal of Magnetism and Magnetic Materials

journal homepage: www.elsevier.com/locate/jmmm

Research articles

Estimating saturation magnetization of superparamagnetic nanoparticles in liquid phase

Kai Wu[a], Diqing Su[b], Jinming Liu[a], Jian-Ping Wang[a,*]

[a] Department of Electrical and Computer Engineering, University of Minnesota, Minneapolis, MN 55455, USA
[b] Department of Chemical Engineering and Material Science, University of Minnesota, Minneapolis, MN 55455, USA

ARTICLE INFO

Keywords:
Superparamagnetic nanoparticle
Saturation magnetization
Langevin function
Ferrofluid

ABSTRACT

Superparamagnetic nanoparticles (SPMNPs), with unique physical and magnetic properties that differentiate them from their bulk magnetic materials, have been widely studied for potential applications in biomedical areas. With proper surface chemical functionalization, SPMNPs have found their applications in magnetic hyperthermia therapy, magnetic bioassays, drug delivery, magnetic manipulation, etc. These applications require elaborate tuning of the physical and magnetic properties of the SPMNPs such as saturation magnetization M_s and magnetic core size D. In this work, we present a search coil-based method to directly characterize the M_s of SPMNPs in the liquid phase. The nonlinear magnetic responses of SPMNPs under oscillating magnetic fields are exploited and the induced harmonic signals are used to analyze their M_s and D. Different combinations of M_s and D are assumed and their harmonic ratios R are summarized. Curve fitting shows that the harmonic ratio $R = 0.74 + 2.85 \times 10^9 \cdot D^{-4.41} \cdot M_s^{-1.44}$, with the coefficient of determination *R-square* = 0.98.

1. Introduction

Superparamagnetic nanoparticle (SPMNP) is an important nanomaterial that has been successfully applied in different biomedical areas such as hyperthermia therapy [1–6], drug delivery [3,7–11], magnetic manipulation and separation [12–16], magnetic biosensing [17–20], etc. In these applications, it is important to tune the magnetic properties of SPMNPs such as saturation magnetization M_s and the physical properties such as magnetic core size D. Herein, we report a search coil-based method for characterizing M_s and D of SPMNPs directly from liquid phase. The nonlinear magnetic responses of SPMNPs to external magnetic fields are unique for different types of SPMNPs regarding their M_s and D, and their response curves are described by the Langevin function. By placing SPMNPs under oscillating magnetic fields, the nonlinear magnetic responses induce odd harmonics that can be picked up by a pair of pick-up coils [21–24]. These harmonic signals contain the information about SPMNPs such as M_s and D [25–28].

As shown in Fig. 1(a), in a typical search coil system, two alternating currents (AC) are applied to outer coils 1 and 2, respectively, and two oscillating magnetic fields are generated inside each coil, respectively (see Fig. 1(a):(i) & (a):(ii)), one with high frequency f_H but small amplitude, the other with low frequency f_L but large amplitude (see Fig. 1(c)) [25,27,28]. The low frequency field periodically drives SPMNPs to saturation where harmonic signals are induced due to the nonlinear magnetic responses of SPMNPs (see Fig. 1(b)). In order to increase the signal-to-noise ratio (SNR), the high frequency field is applied to modulate harmonic signals into the high frequency region where the pink noise (1/f noise) is minimized. A pair of differentially winded pick-up coils (Fig. 1(a):(iii)) is placed in the center of two outer coils, the top half is winded clockwise while the lower half is counterclockwise in order to cancel out the magnetic fields that come from two outer coils. During the measurement, SPMNP ferrofluid sample is confined in a tube and inserted in the upper half of pick-up coils (Fig. 1(a):(iv)), by canceling out the externally applied magnetic fields, this pair of pick-up coils can specifically pick the harmonic signals generated by SPMNPs.

2. Methods

2.1. Theoretical models

Under an external magnetic field, the magnetic moments of SPMNPs tend to align along the applied magnetic field, leading to a net magnetization. The magnetic response of an assembly of SPMNPs is a reversible S-shaped curve modeled by the Langevin function (in emu/cm^3):

$$M_D = M_s L(\xi) \tag{1}$$

* Corresponding author.
E-mail address: jpwang@umn.edu (J.-P. Wang).

https://doi.org/10.1016/j.jmmm.2018.10.008
Received 23 June 2018; Received in revised form 22 August 2018; Accepted 1 October 2018
Available online 03 October 2018
0304-8853/

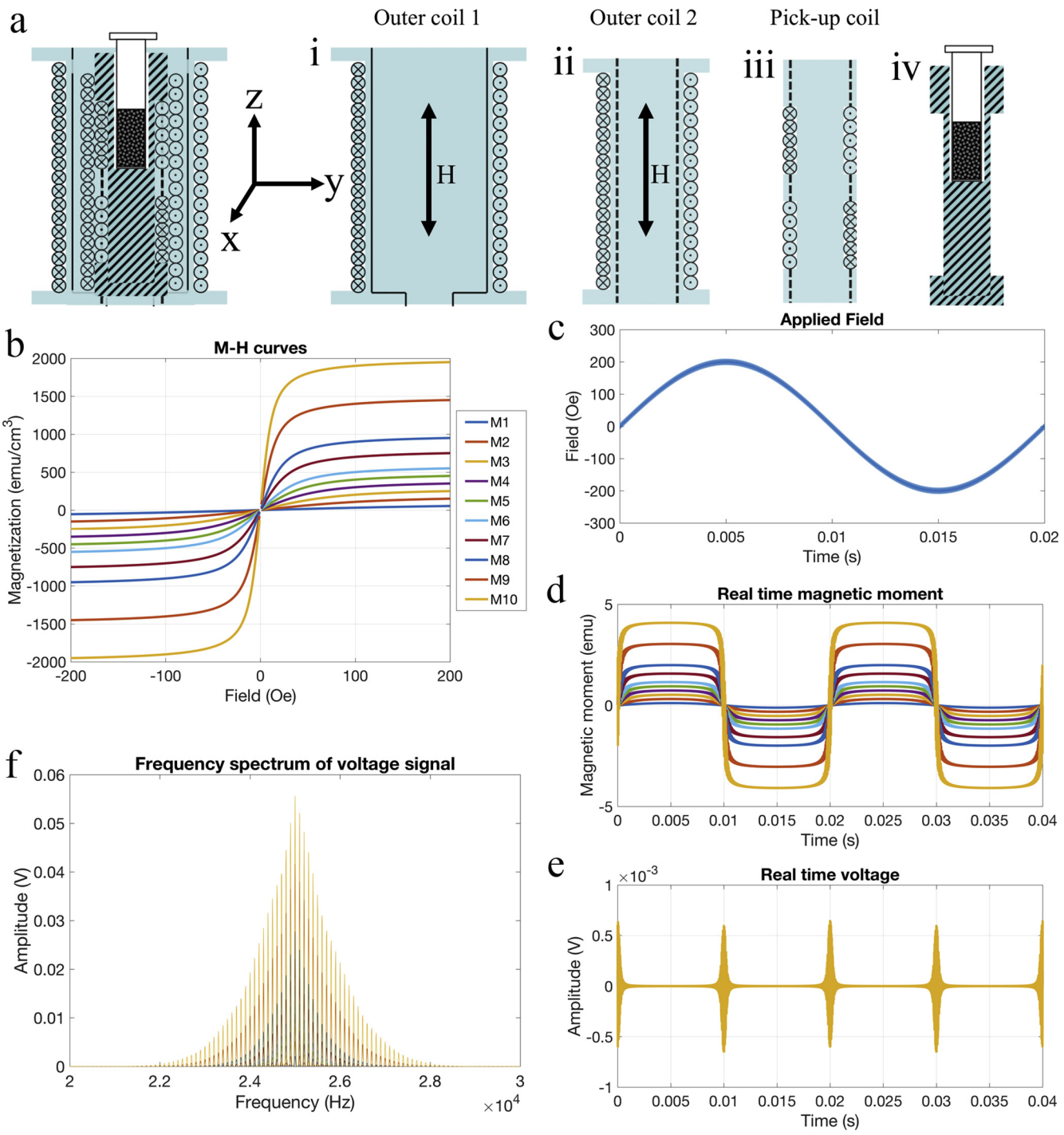

Fig. 1. (a) Search coil system setup. Two oscillating magnetic fields are generated by part (i) and (ii). Part (iii) is a pair of differentially winded pick-up coils, half of the coils are winded clockwise and the other half counter-clockwise to cancel out the external magnetic field from (i) & (ii). Part (iv) is a holder with a plastic tube containing liquid SPMNP sample. (b) Simulated magnetic response curves of 10 SPMNP samples M1–M10 with saturation magnetizations varying from 100 to 2000 emu/cm^3, assuming $D = 20$ nm, and $T = 300$ K. (c) Two oscillating magnetic fields in one $1/f_L$ period. Where $A_L = 200$ *Oe*, $f_L = 50$ Hz, $A_H = 10$ *Oe*, $f_H = 25$ kHz. (d) and (e) are the simulated magnetic moment and induced voltage from 10 SPMNP samples during two $1/f_L$ periods, respectively. Assuming $c = 500$ pM, $V = 0.5$ mL, $D = 20$ nm, $T = 300$ K. (f) Frequency spectrum of (e) shows odd harmonic signals at $f_H \pm 2nf_L$, where n is an integer.

and,

$$L(\xi) = \coth(\xi) - \frac{1}{\xi} \tag{2}$$

$$\xi = \frac{m_s H}{k_B T} \tag{3}$$

$$m_s = M_s V_c = M_s \pi D^3/6 \tag{4}$$

where D and V_c are the magnetic core diameter and magnetic core volume of SPMNP, m_s and M_s are the magnetic moment and saturation magnetization, respectively, H is the external magnetic field, k_B is Boltzmann constant, and T is temperature. Fig. 1(b) shows the simulated magnetic response curves of 10 SPMNPs based on the Langevin model, the M_s of 10 SPMNP samples varies from 100 to 2000 emu/cm^3, assuming $D = 20$ nm, and $T = 300$ K.

Herein, we apply two oscillating magnetic fields to SPMNPs, one

Table 1
Parameters and values in this simulation.

Parameter	Values
High frequency field f_H (kHz)	5–25
High frequency field A_H (Oe)	10
Low frequency field f_L (Hz)	50
Low frequency field A_L (Oe)	50, 100, 150, 200, 250
Pick-up coil radius R (mm)	1.5
Pick-up coil windings	1000
Cross-sectional area of pick-up coils S (mm^2)	π•1.5^2
Average distance from SPMNPs to pick-up coils r' (mm)	1
Sampling rate F_s (kHz)	100
Temperature T (K)	280, 300, 320
SPMNP concentration c (pM)	1, 500, 1000
SPMNP volume V (mL)	0.1, 0.5, 1
SPMNP diameter D (nm)	10, 20, 30
Saturation magnetizations M_s (emu/cm^3) of 10 SPMNPs	100 (M1), 200 (M2), 300 (M3), 400 (M4), 500 (M5), 600 (M6), 800 (M7), 1000 (M8), 1500 (M9), 2000 (M10)

with low frequency f_L but large amplitude A_L, the other with high frequency f_H but small amplitude A_H (see Fig. 1(c)), the overall magnetic field is along z-axis and is expressed as:

$$\vec{H}(t) = [A_H\cos(2\pi f_H t) + A_L\cos(2\pi f_L t)]\hat{z} \tag{5}$$

Taylor expansion of the $M_D(t)$ shows the major mixing frequency components (harmonic signals) due to the nonlinear magnetic responses of SPMNPs:

$$\begin{aligned}\frac{\vec{M}_D(t)}{M_s} &= L\left(\frac{m_s\vec{H}(t)}{k_BT}\right) = \frac{1}{3}\left(\frac{m_s}{k_BT}\right)\vec{H}(t) - \frac{1}{45}\left(\frac{m_s}{k_BT}\right)^3\vec{H}(t)^3 \\ &+ \frac{2}{945}\left(\frac{m_s}{k_BT}\right)^5\vec{H}(t)^5 + \cdots = \cdots + \left[-\frac{1}{60}A_HA_L^2\left(\frac{m_s}{k_BT}\right)^3\right. \\ &\left. + o\left(\left(\frac{m_s}{k_BT}\right)^3\right)\right] \times \cos[2\pi(f_H \pm 2f_L)t]\hat{z} \\ &+ \left[\frac{1}{1512}A_HA_L^4\left(\frac{m_s}{k_BT}\right)^5 + o\left(\left(\frac{m_s}{k_BT}\right)^5\right)\right] \times \cos[2\pi(f_H \pm 4f_L)t]\hat{z} \\ &+ \cdots\end{aligned} \tag{6}$$

Fig. 1(d) shows the simulated magnetic responses of 10 different kinds of SPMNPs based on Langevin model.

Assuming an assembly of SPMNPs with diameter D, total volume of V, and concentration of c, is confined in a cylindrical tube inside a pair of pick-up coils (see Fig. 1(a):(iii)), the total magnetic moment from the ferrofluid sample containing the 3rd and the 5th harmonic components is expressed as (in emu/mL):

$$\begin{aligned}\vec{m}_D(t)|_{3rd} \approx m_scV &\left[-\frac{1}{60}A_HA_L^2\left(\frac{m_s}{k_BT}\right)^3 + o\left(\left(\frac{m_s}{k_BT}\right)^3\right)\right] \\ &\times \cos[2\pi(f_H + 2f_L)t]\hat{z}\end{aligned} \tag{7}$$

$$\begin{aligned}\vec{m}_D(t)|_{5th} \approx m_scV &\left[\frac{1}{1512}A_HA_L^4\left(\frac{m_s}{k_BT}\right)^5 + o\left(\left(\frac{m_s}{k_BT}\right)^5\right)\right] \\ &\times \cos[2\pi(f_H + 4f_L)t]\hat{z}\end{aligned} \tag{8}$$

The dipolar fields generated by magnetized SPMNPs are picked up by a pair of pick-up coils that are only sensitive to the z-direction field, which can be expressed as (in A/m):

$$\mu_0\vec{H}(t)|_{3rd} = \frac{\mu_0}{4\pi}\left(\frac{3\vec{r}\,(\vec{m}_D(t)|_{3rd}\cdot\vec{r})}{r^5} - \frac{\vec{m}_D(t)|_{3rd}}{r^3}\right) \tag{9}$$

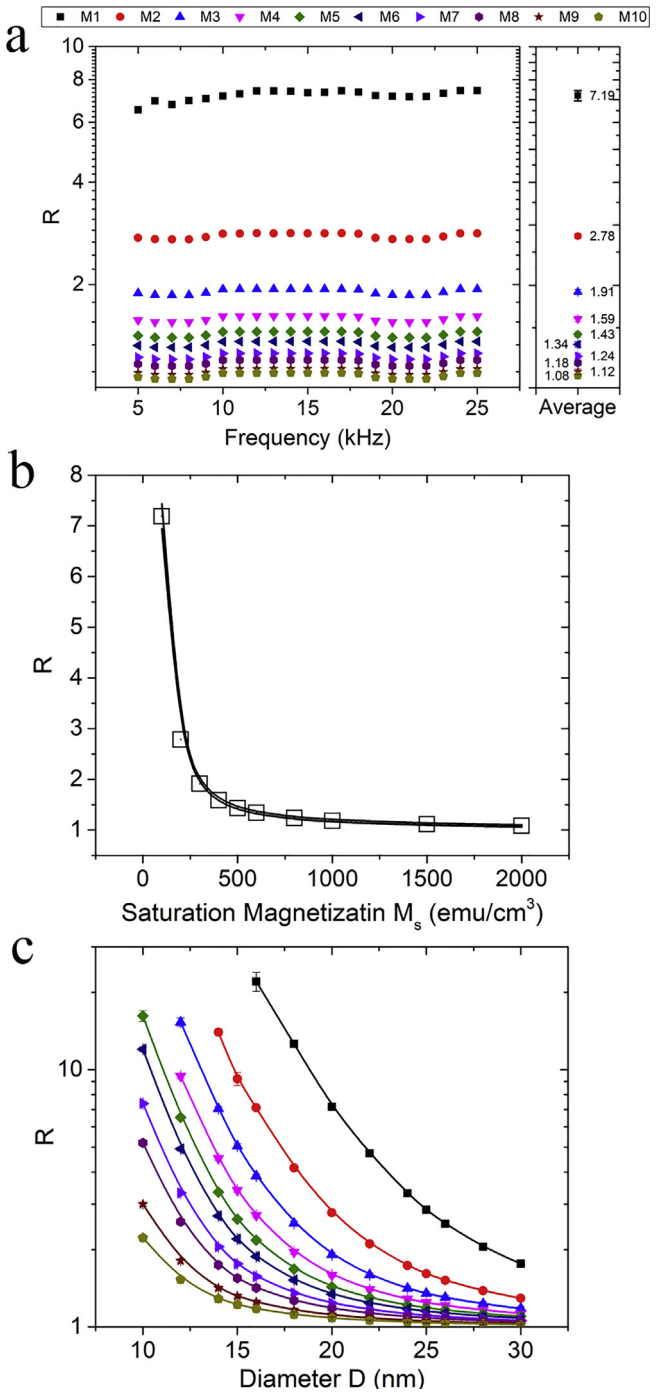

Fig. 2. (a) Harmonic ratio R of 10 SPMNP samples under varying f_H from 5 to 25 kHz. R is independent of f_H. The averaged R values from M1–M10 are plotted on the right side. (b) Harmonic ratio R monotonically decreases as the M_s increases. (c) Averaged harmonic ratio R of 10 SPMNP samples with varying D from 10 to 30 nm.

$$\mu_0\vec{H}(t)|_{5th} = \frac{\mu_0}{4\pi}\left(\frac{3\vec{r}\,(\vec{m}_D(t)|_{5th}\cdot\vec{r})}{r^5} - \frac{\vec{m}_D(t)|_{5th}}{r^3}\right) \tag{10}$$

where $\vec{r}$ is the vector from SPMNP magnetic dipole to the pick-up coils, and μ_0 is the vacuum permeability. By assuming r' is the average distance from SPMNPs to pick-up coils, a simplified form of total dipolar field is expressed as (in A/m):

$$\mu_0\vec{H}(t)|_{3rd} = \frac{\mu_0}{2\pi r'^3}\vec{m}_D(t)|_{3rd} \tag{11}$$

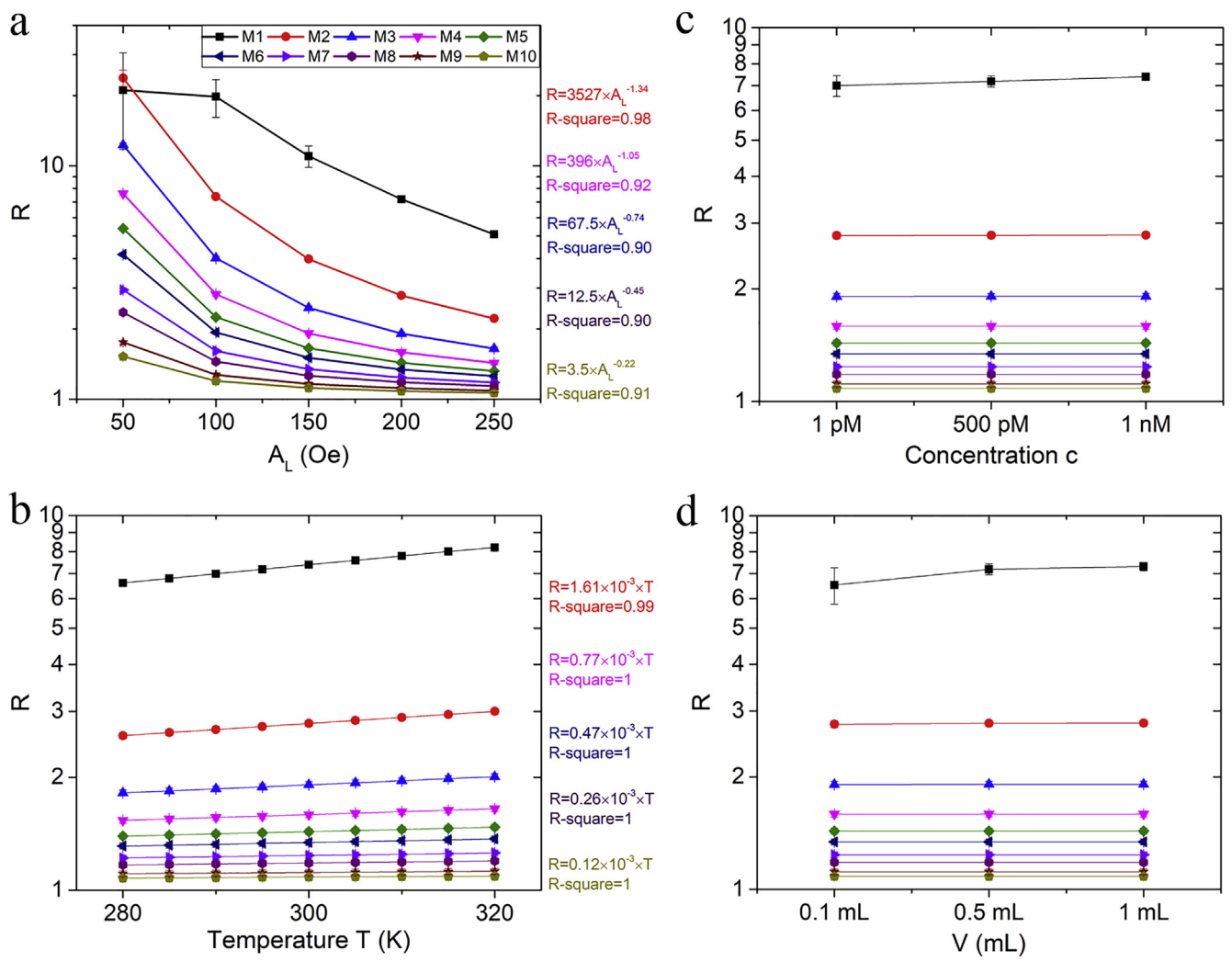

Fig. 3. (a) Averaged harmonic ratio R of 10 SPMNP samples under varying A_L from 50 to 250 Oe. Assuming c = 500 pM, V = 0.5 mL, T = 300 K, D = 20 nm. Harmonic ratio R monotonically decreases as A_L increases obeying $R = j \times {A_L}^{-k}$, where the values of j and k are constants that depend on M_s. Curve fitting on the R versus A_L for M2, M4, M6, M8, and M10 are summarized. With the diameter D fixed, j and k monotonically increase as M_s increases. (b) Averaged harmonic ratio R of 10 SPMNP samples under varying T from 280 K to 320 K, assuming c = 500 pM, V = 0.5 mL, A_L = 200 Oe, D = 20 nm. Harmonic ratio R monotonically increases as T increases obeying $R = l \times T$, where l is a constant that depends on M_s. Curve fitting results on the R versus T for M2, M4, M6, M8, and M10 are summarized. (c) Harmonic ratio R is independent of concentration c. (d) Harmonic ratio R is independent of sample volume V.

$$\mu_0 \vec{H}(t)|_{5th} = \frac{\mu_0}{2\pi {r'}^3} \vec{m}_D(t)|_{5th} \tag{12}$$

According to Faraday's law, the induced time-varying harmonic voltages sensed by pick-up coils are (in V):

$$u(t)|_{3rd} = -NS \frac{d(\mu_0 \vec{H}(t)|_{3rd})}{dt} \tag{13}$$

$$u(t)|_{5th} = -NS \frac{d(\mu_0 \vec{H}(t)|_{5th})}{dt} \tag{14}$$

where N is the number of winding turns, S is the area contained by the pick-up coils.

Fig. 1(e) shows the induced voltage signals from 10 SPMNP samples that are sensed by the pick-up coils. By performing the nonequispaced fast Fourier transform (NFFT) on the voltage signals, the frequency spectrum is extracted and plotted in Fig. 1(f). In this paper, we analyzed the 3rd ($f_H \pm 2f_L$) and 5th ($f_H \pm 4f_L$) harmonic signals. The amplitude ratio of the 3rd over the 5th harmonics (R) was used to analyze M_s and D [29].

By neglecting the higher order smaller components $o\left(\left(\frac{m_s}{k_B T}\right)^3\right)$ and $o\left(\left(\frac{m_s}{k_B T}\right)^5\right)$ in Eqs. (7) and (8), the estimated amplitude ratio of the 3rd over the 5th harmonics reduces to:

$$R \propto \frac{f_H + 2f_L}{f_H + 4f_L} \cdot \frac{k_B T}{{A_L}^2 {M_s}^2 D^6} \tag{15}$$

Since f_H is at least 20 times larger than f_L, the above equation reduces to:

$$R \propto \frac{k_B T}{{A_L}^2 {M_s}^2 D^6} \tag{16}$$

The foregoing theoretical derivations are very simplified but it's very useful to know what parameters are affecting the harmonic ratio R. Theoretically, the harmonic ratio is negatively correlated with the magnetic core diameter D, saturation magnetization M_s, and amplitude of the driving field A_L. Another advantage of using harmonic ratio R to characterize the magnetic properties of SPMNPs is that this parameter is independent of concentration c and volume V of SPMNP ferrofluid samples.

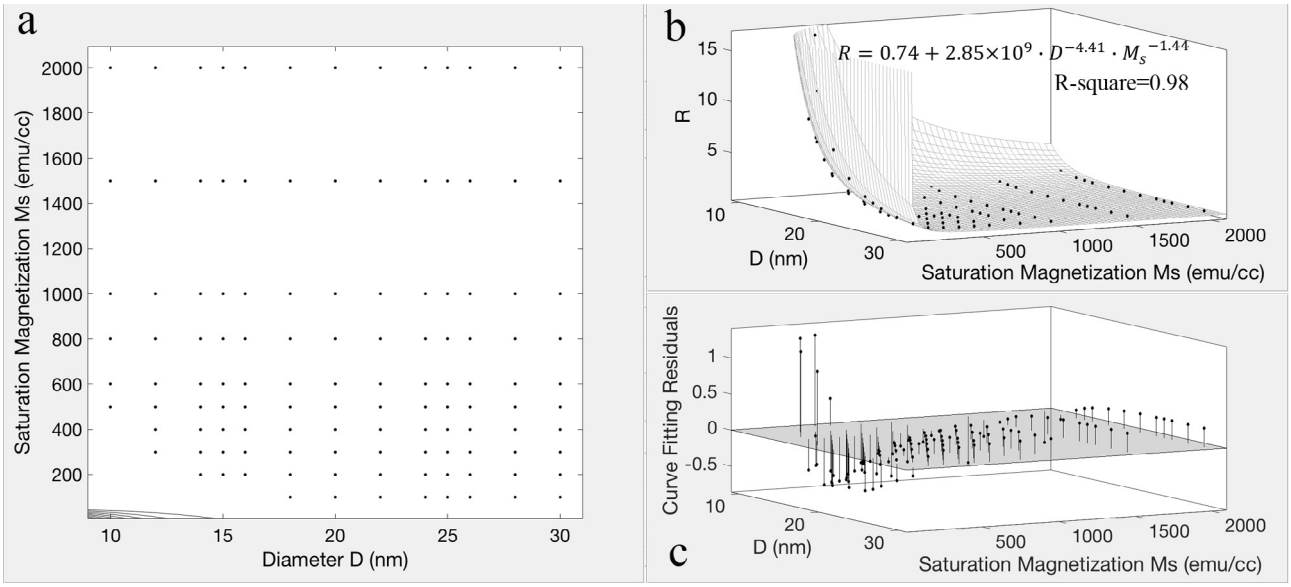

Fig. 4. (a) Harmonic ratios R are collected from SPMNPs with different combinations of D and M_s. Assuming $T = 300$ K, $A_L = 200$ *Oe*. Each point represents one combination of D and M_s. (b) R values as function of D and M_s. Curve fitting shows$R$ obeys the trend $R = m + n{\bullet}D^{p}{\bullet}M_s^{q}$, where m, n, p, and q are constants that dependent on A_L and T. The surface equation in (b) is $R = 0.74 + 2.85 \times 10^{9}{\bullet}D^{-4.41}{\bullet}M_s^{-1.44}$. Each point represents R value at one combination of D and M_s. (c) Curve fitting residuals from (b).

Table 2
Coefficient values and 95% confidence bounds in Eq. (17).

Coefficient	Value	95% confidence bounds
m	0.7413	(0.6262, 0.8563)
n	2.852×10^{9}	$(1.661 \times 10^{8}, 5.538 \times 10^{9})$
p	4.408	(4.196, 4.62)
q	1.443	(1.369, 1.518)

2.2. Simulation design

In this simulation, SPMNPs are assigned with different diameters D and saturation magnetizations M_s. At the same time, ferrofluid samples are assigned with varying concentrations c and volumes V. Their magnetic responses are recorded under different driving magnetic field frequencies f_H, amplitudes A_L and temperatures T. These parameters and values used in this paper are listed in Table 1.

The Langevin model in Eq. (1) is used in this simulation. By putting the time varying magnetic field$\vec{H}(t)$, different combinations of M_s, D, V, c, and T in this equation, the real-time magnetic response data are collected. With the search coil parameters assumed (see Table 1), the Faraday's law is applied to calculate the real-time voltage in the pick-up coils. Finally, the amplitudes of the 3rd and the 5th harmonics, as well as the harmonic ratio R, are collected by performing NFFT on real-time voltage.

3. Results and discussion

3.1. Harmonic ratio R versus M_s andD

In this section, different SPMNP samples with varying M_s and D are studied. By sweeping the high frequency field f_H from 5 to 25 kHz, the harmonic ratios R are collected. By assuming $c = 500$ pM, $V = 0.5$ mL, $D = 20$ nm, $T = 300$ K, and $A_L = 200$ *Oe*, the harmonic ratios R from 10 SPMNP samples (M1–M10, with M_s varies from 100 to 2000 emu/cm^3, see details in Table 1) are plotted in Fig. 2(a). Harmonic ratio R is independent of f_H and it decreases monotonically as M_s increases (see Fig. 2(b)). Furthermore, we varied SPMNP diameters D from 10 to 30 nm and collected the averaged R values for M1–M10. Fig. 2(c) shows that: 1) for SPMNPs with the same size D, a higher R value indicates a lower M_s, 2) for SPMNPs with the same M_s, higher R-value indicates a smaller magnetic core diameter D.

3.2. Harmonic ratio R versus A_L, T, c, and V

Theoretical analysis from Eq. (16) shows that harmonic ratio R is dependent on several parameters excluding M_s and D, such as the amplitude of low frequency field A_L and the temperature T. The SPMNP sample concentration c and total volume V both affect the magnitudes of harmonic signals, although these parameters are not affecting the harmonic ratio R as seen in Eq. (16). In Fig. 3(a), we varied A_L from 50 to 250 Oe and plotted R versus A_L for M1–M10 samples while setting other parameters fixed. These curves clearly show that R is proportional to A_L^{-k} (k is a constant that depends on the M_s of SPMNPs), which agrees well with our theoretical model. In Fig. 3(b), we varied T from 280 K to 320 K and the R versus T curves clearly show that R is linearly proportional to T, which agrees with our theoretical model. Harmonic ratios R are also summarized for SPMNP samples with different concentrations c and volumes V and plotted in Fig. 3(c) and (d), which clearly shows that R is independent of c and V.

3.3. Curving fitting on $R = f(D, M_s)$

The foregoing sections demonstrated that the harmonic ratio R is dependent on M_s, D, A_L, and T, but is independent of c and V. In most applications, A_L and T can be artificially fixed as constants. Herein, we assume the driving field amplitude is set to be $A_L = 200$ *Oe*, and the temperature is set to $T = 300$ K. As shown in Fig. 4(a), SPMNP samples with different combinations of M_s and D are studied and averaged harmonic ratios R are collected by sweeping f_H from 5 to 25 kHz. We plotted R versus M_s and D in Fig. 4(b). The MATLAB curve fitting shows that R obeys the following equation:

$$R = m + n{\bullet}D^{p}{\bullet}M_s^{q} \tag{17}$$

where the coefficients m, n, p, and q are constants that dependent on A_L and T. The values of these coefficients are listed in Table 2. By applying $R = 0.74 + 2.85 \times 10^{9}{\bullet}D^{-4.41}{\bullet}M_s^{-1.44}$, the curve fitting residuals at different combinations of M_s and D are plotted in Fig. 4(c).

4. Conclusions

In this work, we have proposed and demonstrated a search coil-based method to directly characterize the M_s and D of SPMNPs in liquid phase for the first time. SPMNPs have been extensively used as bio-imaging contrast agents, heating sources for tumor therapy, and carriers for controlled drug delivery and release to target organs and tissues. All of these applications require elaborate tuning of the physical and magnetic properties of the SPMNPs. The nonlinear magnetic responses of SPMNPs were analyzed and, by applying two oscillating magnetic fields to periodically drive SPMNPs to saturation, we have successfully analyzed the harmonic signals that are unique for each type of SPMNP regarding its M_s and D. Theoretical models in Section 2.1 point out that the harmonic ratio R is proportional to temperature T and negatively correlated with A_L, M_s, and D, and it's independent of SPMNP ferrofluid concentration c and volume V. In Sections 3.1 and 3.2, mathematical simulations were carried out conforming the real search coil setup dimensions and today's SPMNP properties. It was confirmed that harmonic ratio R is linearly proportional to temperature T, and monotonically decreases as the A_L increases. In Section 3.3, by fixing the A_L and T, we have successfully curve-fitted $R = f(D, M_s)$ by collecting the R values from different combinations of M_s and D. The results in Fig. 4 shows that $R = 0.74 + 2.85 \times 10^9 \bullet D^{-4.41} \bullet M_s^{-1.44}$ with the coefficient of determination $R\text{-}square = 0.98$.

Herein, we stress the feasibility of using search coils as a method to characterize the physical and magnetic properties of SPMNPs, which may be applied as building blocks in nanoparticle characterization devices.

Acknowledgements

This work is supported by Institute of Engineering in Medicine of the University of Minnesota, National Science Foundation MRSEC facility program, the Distinguished McKnight University Professorship, Centennial Chair Professorship, Robert F Hartmann Endowed Chair, and UROP program from the University of Minnesota.

Appendix A. Supplementary data

Supplementary data to this article can be found online at https://doi.org/10.1016/j.jmmm.2018.10.008.

References

[1] I. Andreu, E. Natividad, L. Solozábal, O. Roubeau, Nano-objects for addressing the control of nanoparticle arrangement and performance in magnetic hyperthermia, ACS Nano 9 (2) (2015) 1408–1419.
[2] M. Bañobre-López, A. Teijeiro, J. Rivas, Magnetic nanoparticle-based hyperthermia for cancer treatment, Rep. Pract. Oncol. Radiother. 18 (6) (2013) 397–400.
[3] P. Biehl, M. von der Luhe, S. Dutz, F.H. Schacher, Synthesis, characterization, and applications of magnetic nanoparticles featuring polyzwitterionic coatings, Polymers 10 (1) (2018) 28. Art. no. 91.
[4] R. Hergt, S. Dutz, Magnetic particle hyperthermia—biophysical limitations of a visionary tumour therapy, J. Magn. Magn. Mater. 311 (1) (2007) 187–192.
[5] S. Laurent, S. Dutz, U.O. Häfeli, M. Mahmoudi, Magnetic fluid hyperthermia: focus on superparamagnetic iron oxide nanoparticles, Adv. Colloid Interface Sci. 166 (1) (2011) 8–23.
[6] K. Wu, J.-P. Wang, Magnetic hyperthermia performance of magnetite nanoparticle assemblies under different driving fields, AIP Adv. 7 (5) (2017) 056327.
[7] M. Arruebo, R. Fernández-Pacheco, M.R. Ibarra, J. Santamaría, Magnetic nanoparticles for drug delivery, Nano Today 2 (3) (2007) 22–32.
[8] G. Bao, S. Mitragotri, S. Tong, Multifunctional nanoparticles for drug delivery and molecular imaging, Annu. Rev. Biomed. Eng. 15 (2013) 253–282.
[9] S. Laurent, A.A. Saei, S. Behzadi, A. Panahifar, M. Mahmoudi, Superparamagnetic iron oxide nanoparticles for delivery of therapeutic agents: opportunities and challenges, Exp. Opin. Drug Deliv. 11 (9) (2014) 1449–1470.
[10] S.C. McBain, H.H. Yiu, J. Dobson, Magnetic nanoparticles for gene and drug delivery, Int. J. Nanomed. 3 (2) (2008) 169.
[11] C. Sun, J.S. Lee, M. Zhang, Magnetic nanoparticles in MR imaging and drug delivery, Adv. Drug Deliv. Rev. 60 (11) (2008) 1252–1265.
[12] Q. Chen, et al., Fast and sensitive detection of foodborne pathogen using electrochemical impedance analysis, urease catalysis and microfluidics, Biosens. Bioelectron. 86 (2016) 770–776.
[13] J. He, M. Huang, D. Wang, Z. Zhang, G. Li, Magnetic separation techniques in sample preparation for biological analysis: a review, J. Pharm. Biomed. Anal. 101 (2014) 84–101.
[14] I. Herrmann, A. Schlegel, R. Graf, W.J. Stark, B. Beck-Schimmer, Magnetic separation-based blood purification: a promising new approach for the removal of disease-causing compounds? J. Nanobiotechnol. 13 (1) (2015) 49.
[15] M. Shao, F. Ning, J. Zhao, M. Wei, D.G. Evans, X. Duan, Preparation of Fe_3O_4@SiO_2@ layered double hydroxide core–shell microspheres for magnetic separation of proteins, JACS 134 (2) (2012) 1071–1077.
[16] Y.L. Wang, S. Ravindranath, J. Irudayaraj, Separation and detection of multiple pathogens in a food matrix by magnetic SERS nanoprobes, Anal. Bioanal. Chem. 399 (3) (Jan 2011) 1271–1278.
[17] J. Choi, A.W. Gani, D.J.B. Bechstein, J.R. Lee, P.J. Utz, S.X. Wang, Portable, one-step, and rapid GMR biosensor platform with smartphone interface, Biosens. Bioelectron. 85 (2016) 1–7.
[18] A.V. Orlov, et al., Magnetic immunoassay for detection of staphylococcal toxins in complex media, Anal. Chem. 85 (2) (2013/01/15 2013.) 1154–1163.
[19] X.C. Sun, C. Lei, L. Guo, Y. Zhou, Separable detecting of Escherichia coli O157H:H7 by a giant magneto-resistance-based bio-sensing system, Sens. Actuators B: Chem. 234 (2016) 485–492.
[20] H. Wang, Y. Li, A. Wang, M. Slavik, Rapid, sensitive, and simultaneous detection of three foodborne pathogens using magnetic nanobead-based immunoseparation and quantum dot-based multiplex immunoassay, J. Food. Prot. 74 (12) (2011) 2039–2047.
[21] A.M. Rauwerdink, J.B. Weaver, Harmonic phase angle as a concentration-independent measure of nanoparticle dynamics, Med. Phys. 37 (6) (2010) 2587–2592.
[22] J.B. Weaver, M. Harding, A.M. Rauwerdink, E.W. Hansen, The effect of viscosity on the phase of the nanoparticle magnetization induced by a harmonic applied field, pp. 762627-762627-8, SPIE Medical Imaging, International Society for Optics and Photonics, 2010.
[23] X. Zhang, et al., Molecular sensing with magnetic nanoparticles using magnetic spectroscopy of nanoparticle Brownian motion, Biosens. Bioelectron. 50 (2013) 441–446.
[24] K. Wu, L. Tu, D. Su, J.-P. Wang, Magnetic dynamics of ferrofluids: mathematical models and experimental investigations, J. Phys. D Appl. Phys. 50 (8) (2017) 085005.
[25] L. Tu, K. Wu, T. Klein, J.-P. Wang, Magnetic nanoparticles colourization by a mixing-frequency method, J. Phys. D: Appl. Phys. 47 (15) (2014) 155001.
[26] K. Wu, J. Liu, Y. Wang, C. Ye, Y. Feng, J.-P. Wang, Superparamagnetic nanoparticle-based viscosity test, Appl. Phys. Lett. 107 (5) (2015) 053701.
[27] P.I. Nikitin, P.M. Vetoshko, T.I. Ksenevich, New type of biosensor based on magnetic nanoparticle detection, J. Magn. Magn. Mater. 311 (1) (2007) 445–449.
[28] H.-J. Krause, et al., Magnetic particle detection by frequency mixing for immunoassay applications, J. Magn. Magn. Mater. 311 (1) (2007) 436–444.
[29] K. Wu, K. Schliep, X. Zhang, J. Liu, B. Ma, J.P. Wang, Characterizing physical properties of superparamagnetic nanoparticles in liquid phase using Brownian relaxation, Small 13 (22) (2017).